Improved nitrate-to-ammonia electrocatalysis through concerted proton-coupled electron transfer

Guanqiao Yu,[b#] Zilu Guo,[a#] Yuefei Li,[a] Shan Huang,[a*] and Jiayuan Li[a*]

[a]Key Laboratory of Special Functional and Smart Polymer Materials of Ministry of Industry and Information Technology, School of Chemistry and Chemical Engineering, Northwestern Polytechnical University, Xi'an 710072, China.

[b]School of Chemistry and Chemical Engineering,Southwest Petroleum University, China.

Corresponding authors:
Jiayuan Li, E-mail: Jiayuanli@nwpu.edu.cn.
Shan Huang, E-mail: shanhuang@nwpu.edu.cn.

Experimental section

Synthesis of copper foam (CF) modified with phytate functional group (PA-CF). Typically, the bare CF (3 cm × 1 cm) was pre-cleaned by sonication in 5% HCl, acetone, ethanol and deionized (DI) water for 10 min consecutively. Then, the 10.5 ml phytic acid (50% in H_2O, w/w) was added to 70 mL DI water to obtain a transparent solution. Afterwards, the pretreated CF was immersed into the reaction solution and then treated in a Teflon vessel (100 mL) at 120 °C for 10 h. After cooling down to room temperature, the obtained PA-CF was rinsed by water/ethanol alternatively and dried at 60 °C.

Characterization. The scanning electron microscopy (SEM) images were taken with a Hitachi S4800 SEM (Japan, 3 kV). The X-ray diffraction (XRD) patterns of the products were recorded with Bruker D8 Focus Diffraction System using a Cu Kα source (λ = 0.15406 nm). Fourier transform infrared spectroscopy (FT-IR) spectrum was carried out with an MAGNA1IR 750 (Nicolet Instrument Co) FT-IR spectrometer. The attenuated total reflection infrared spectrum (ATR-IR) was characterized by a NICOLET 6700 FTIR spectrophotometer (Thermo Fisher U.S.A.). The X-ray photoelectron spectroscopy (XPS) measurements were performed on a photoelectron spectrometer using Al Kα radiation as the excitation source (PHI 5000 VersaProbe). All the peaks were calibrated with the C1s spectrum at a binding energy of 284.8 eV. The elemental content was analyzed by inductively-coupled plasma mass spectrometry (ICP-MS, Agilent 7500CE).

Electrochemical measurements. Catalytic performance for electrocatalytic NITRR of the various catalysts were investigated by a CHI 760E workstation (CH Instruments, Inc., Shanghai) in a three-electrode H-type cell, where the synthesized catalysts, saturated calomel electrode (SCE) and graphite rod as the working electrode, reference electrode and counter electrode, respectively. The working electrode with the area of 1 × 2 cm^2 was immersed in 0.1 M K_2SO_4 solution (50 mL) with 0.5 M KNO_3 as the reactant for the measurements. Linear sweep voltammetry (LSV) curves for various catalysts with a scan rate of 5 mV s^{-1} were recorded to evaluate their catalytic activities. Accordingly, a potentiostatic test was conducted at the given potential for 1 h with a stirring rate of ~500 rpm to drive the reaction. Electrochemical impedance spectroscopy (EIS) investigations were conducted on the GAMRY Reference 600 electrochemistry workstation in the frequency range of 100 kHz−0.1 Hz at various overpotentials. For electrochemical measurements, all potentials reported herein are relative to the reversible hydrogen electrode (RHE) based on the formula: E(RHE) = E(SCE) + 0.242 V + 0.0591 × pH.[1-3]

Product analysis. The ultraviolet-visible (UV-Vis) absorbance spectra were employed to analyze the NH_3 products. To realize UV-Vis analysis, the color agent was prepared by dissolving salicylic acid (0.1 g) and sodium citrate (0.1 g) into NaOH solution (2 mL, 1.0 M) and then mixing with NaClO solution (1 mL, 0.05 M) and sodium nitroferricyanide solution (0.2 mL, 1.0 wt%). Then, a series of standard NH_4Cl solutions (5 mL) with different NH_4^+ concentrations was mixed with the color agent for 30 min for UV-Vis measurements. The absorption intensity at a wavelength of 654 nm was recorded, providing the corresponding concentration-absorbance curve as shown in Figure S1. Then, the electrolyte in cathodic chamber and gas capture bottle was collected and diluted. The diluted electrolytes (5 mL) were also mixed with the above color agent for UV-Vis detection, and through the obtained value of $A_{654\ nm}$, the concentration of generated NH_3 can be calculated. The gaseous product of electrochemical experiments was collected using a gas bag from and analyzed by GC (North Point Gc 901A), which was equipped with TCD detectors using argon as the carrier gas.

Faraday efficiency (FE) evaluation. The FE of the relevant reactions was calculated as:

$$\mathrm{FE}\ (\%) = n\,\mathrm{F}\,\mathrm{m} / Q$$

where n represents the electron-transfer number, m represents the amount of generated products, F represents the Faradaic constant (96485 C mol^{-1}), and Q is the total charge passed through the electrode.

1. Supplementary Figures

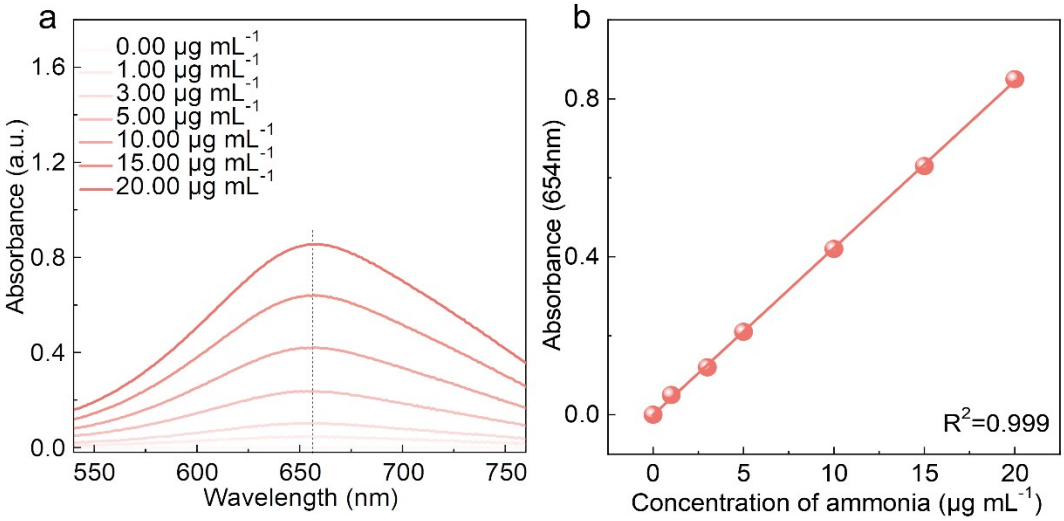

Figure S1. (**a**) Ultraviolet-visible (UV-Vis) absorption spectra of various NH_4^+ concentrations. (**b**) Calibration curve used for estimation of NH_4^+ concentration.

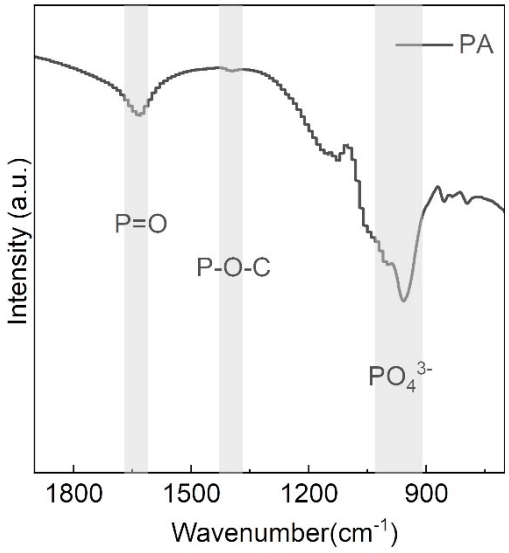

Figure S2. Fourier transform infrared spectroscopy (FT-IR) spectra of the PA benchmarks.

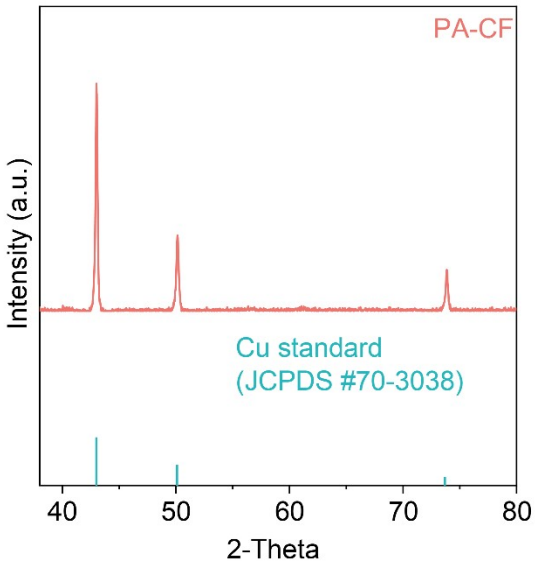

Figure S3. XRD pattern for the PA-CF.

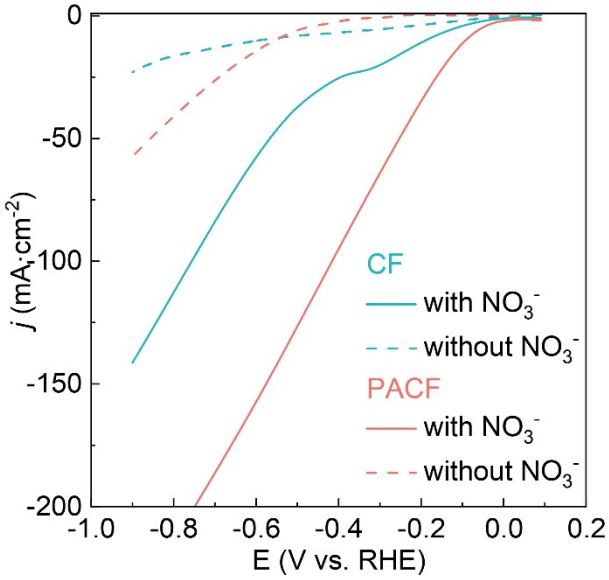

Figure S4. Linear sweep voltammetry (LSV) of the bare CF and PA-CF in 0.1 M K_2SO_4 with and without 0.5 M KNO_3.

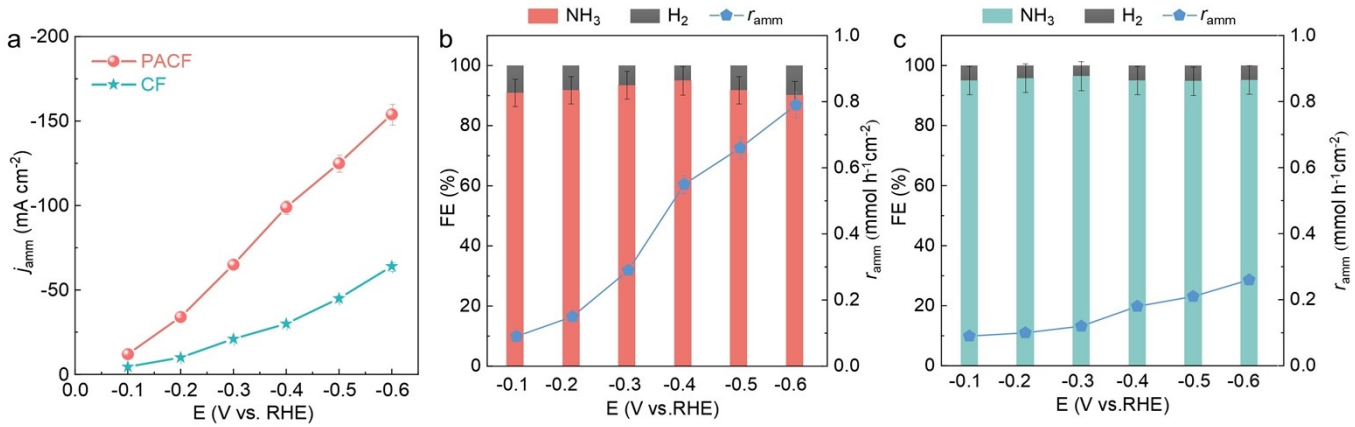

Figure S5. (**a**) Partial current density of CF and PA-CF in 0.1 M K_2SO_4 with and without 0.5 M KNO_3. (**b**) The obtained ammonia yield and FE of PA-CF at different potentials. (**c**) The obtained ammonia yield and FE of CF at different potentials. Error bars stand for the standard deviation of three independent measurements.

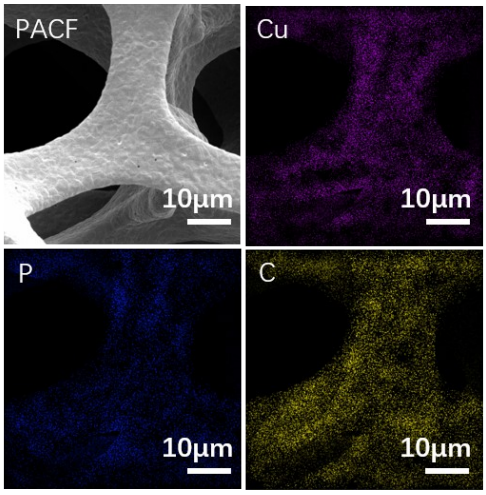

Figure S6. Characterizations of the spent PA-CF catalysts by SEM and EDX.

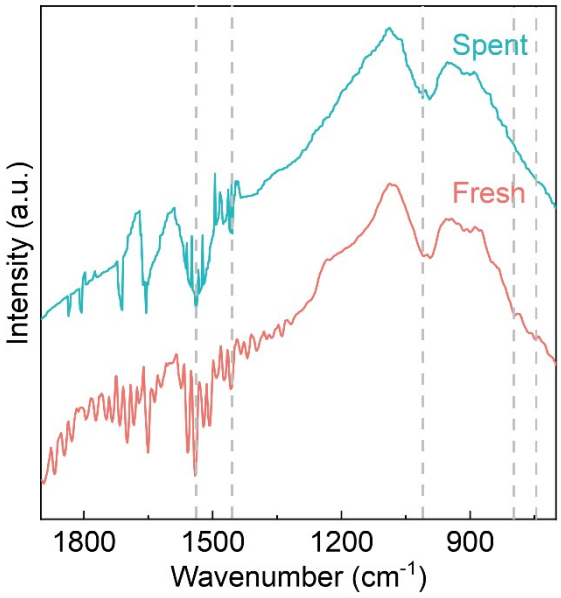

Figure S7. FT-IR spectra of the fresh and spent PA-CF.

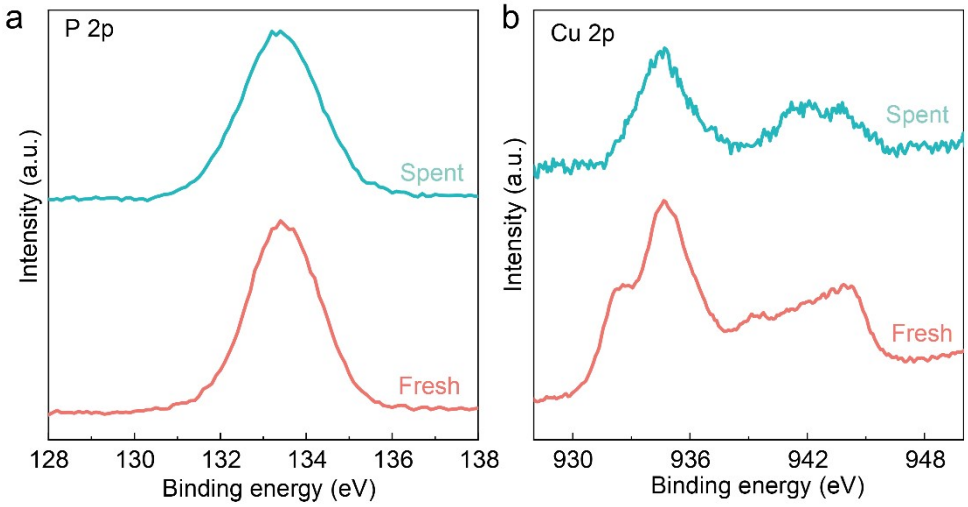

Figure S8. High-resolution XPS spectra of the fresh and spent PA-CF in the (**a**) Cu 2p and (**b**) P 2p region.

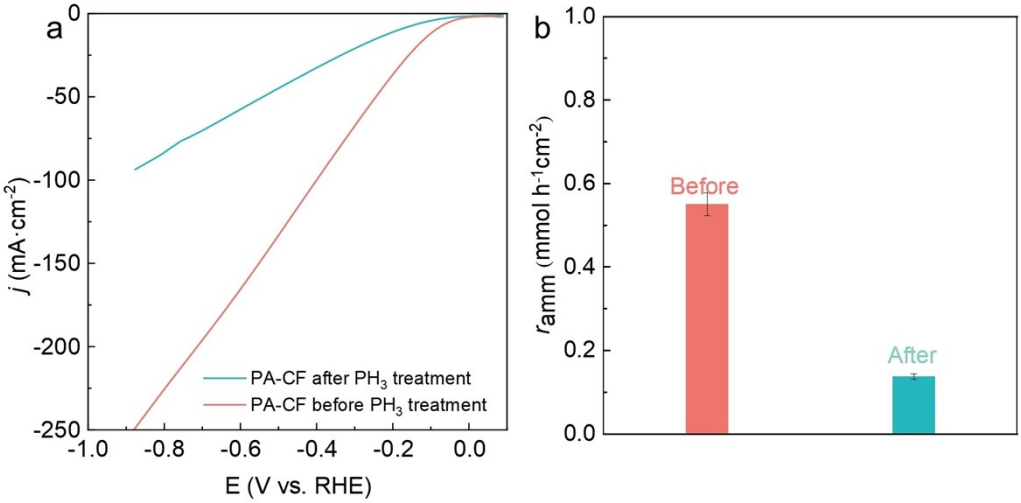

Figure S9. Catalytic performance of the PA-CF before and after PH_3 treatment.

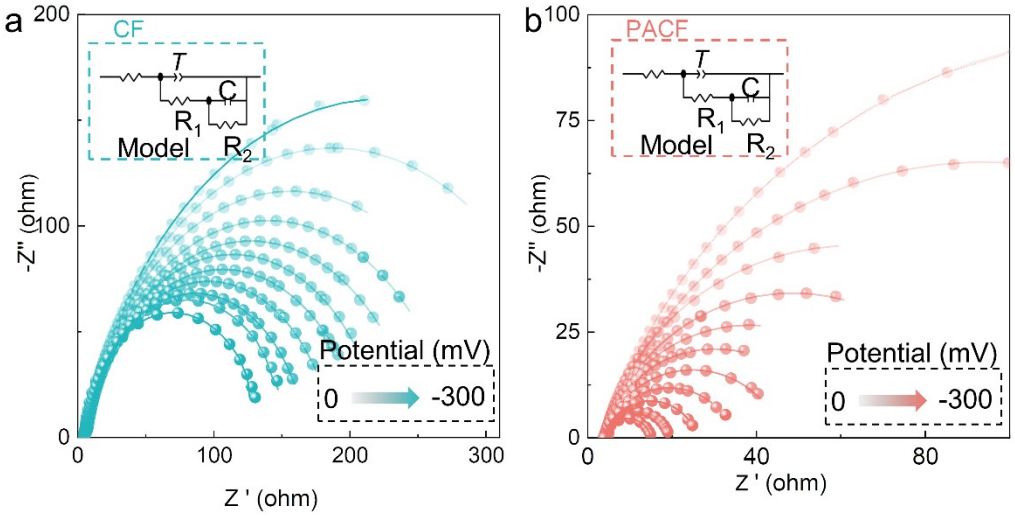

Figure S10. Nyquist plots for the (**a**) CF and (**b**) PA-CF catalysts in 0.1 M K_2SO_4 with0.5 M KNO_3 electrolyte at various NITRR overpotentials. The inset shows the equivalent circuit for the simulation. The scattered symbols represent the experimental results, and the solid lines are the fitted results. The fitted parameters are summarized in Table S3.

2. Estimation of kinetic isotope effects. To estimate the kinetic isotope effects (KIE) of the CF and PA-CF, their cyclic voltammetry (CV) (Figure S11) was investigated in H_2O/K_2SO_4 or D_2O/K_2SO_4 (0.1 M) electrolyte with or without KNO_3 substrate (0.5 M) at various scan rate.

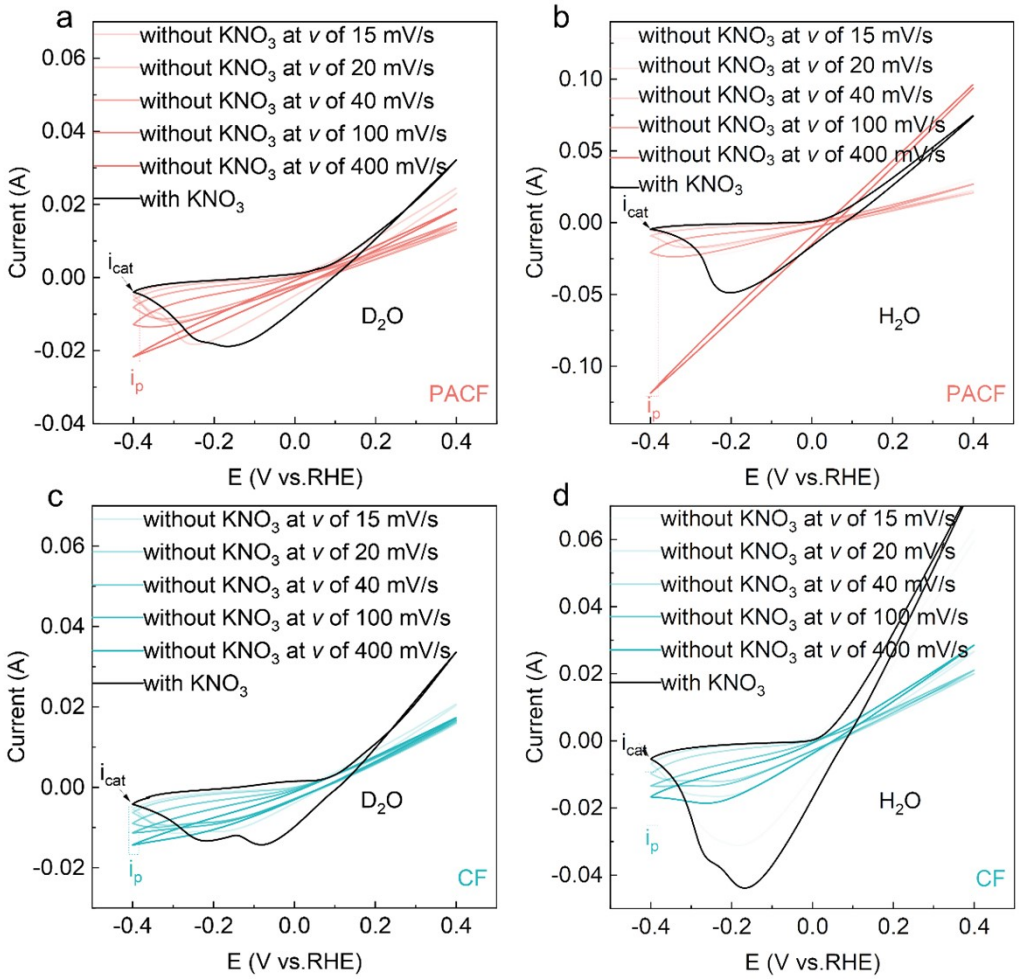

Figure S11. (**a**) CVs of the PA-CF in 0.1 M D_2O/K_2SO_4 electrolyte with or without KNO_3 at various scan rates. (**b**) CVs of the PA-CF in 0.1 M H_2O/K_2SO_4 electrolyte with or without KNO_3 at various scan rates. (**c**) CVs of the CF in 0.1 M D_2O/K_2SO_4 electrolyte with or without KNO_3 at various scan rates. (**d**) CVs of the CF in 0.1 M H_2O/K_2SO_4 electrolyte with or without KNO_3 at various scan rates.

The *k* values can be determined based on the Eq. S1:[4-6]

$$\frac{i_{cat}}{i_p} = 2.24\sqrt{\frac{RT}{Fv}kC_s} \qquad \text{Eq. S1}$$

where i_{cat} is reflected by the maximal current of the corresponding CV measurement with KNO_3 substrate, i_p is reflected by the maximal current of the corresponding CV measurements without KNO_3 substrate, R is the gas constant, T is the temperature, F is the Faraday constant, k is rate constant, C_s is the concentration of the substrate (0.5 M) and v is the scan rate. When using H_2O/K_2SO_4 or D_2O/K_2SO_4 electrolyte, the $k_H^{1/2}$ or $k_D^{1/2}$ were calculated from the slopes of ploting

the corresponding i_{cat}/i_p vs. the $v^{-1/2}$ (Figure 4a in the manuscript). Then, the KIE values were calculated to be 1.35 and 2.43 for the CF and PA-CF.

3. Determination of apparent activation energy

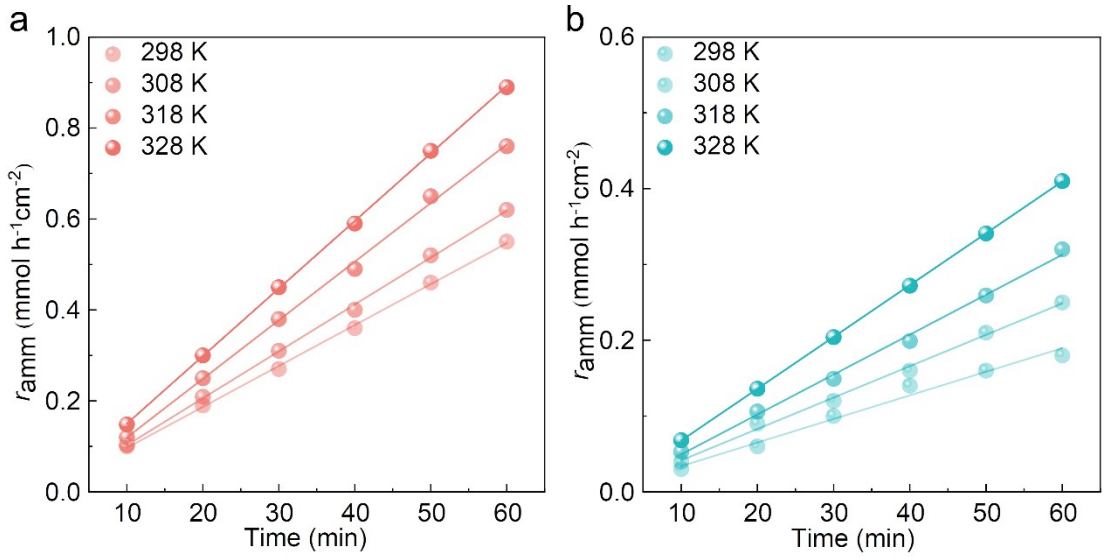

Figure S12. Time-dependent amount of the ammonia yield for the (**a**) PA-CF and (**b**) CF electrodes at different temperatures ranging from 298 to 328 K. The dash lines showed the linearly fitted curves.

4. Determination of the dependence between electron transfer deriving force and electron transfer rate.

As shown in Figure S13-S19, for the NITRR catalyzed by the PA-CF, the electron transfer (ET) rate constants (k_{ET}) of PA-CF at different pH (7.0, 7.2, 7.4, 7.6, 7.8 and 8.0) were calculated from the slope of ploting the apparent reaction rate (k_{obs}) of ET vs. KNO_3 concentrations (C_s) in H_2O/K_2SO_4 electrolyte with tunable KOH concentration according to the Eq. S2 and S3.[4-8]

$$\frac{i_{cat}}{i_p} = 2.24\sqrt{\frac{RT}{Fv}k_{obs}} \qquad \text{Eq. S2}$$

$$k_{obs} = k_{ET}C_s \qquad \text{Eq. S3}$$

On the other hand, the ET driving force $-\Delta G^0_{ET}$ at the above pH (7.0, 7.2, 7.4, 7.6, 7.8 and 8.0) was calculated by the Eq. S4 and S5.[7,8]

$$\Delta G^0_{ET} = e\left(E'_{ox} - E_{red}\right) \qquad \text{Eq. S4}$$

$$E'_{ox} = E_{ox} + 0.0591 \times pH \qquad \text{Eq. S5}$$

Where E_{red} represents the reduction potential and is 0.94 for KNO_3 while E_{ox} represents the oxidation potential and is 0.34 for Cu.[9-11] Based on Figure S13-18, ploting the obtained $-\Delta G^0_{ET}$ vs. ln k_{ET} at the above KOH concentrations (or pH values) gives the $-\Delta G^0_{ET}$ dependence with respect to k_{ET} as shown in Figure 4c in the manuscript.

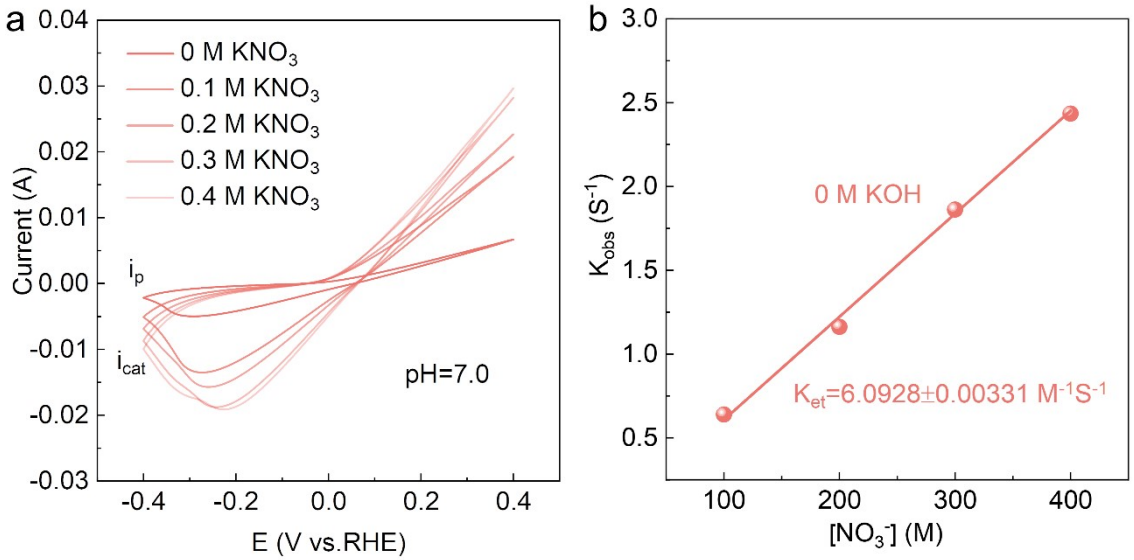

Figure S13. (**a**) CVs of the PA-CF with x M (0, 0.1, 0.2, 0.3, 0.4) KNO_3 at pH=7.0. (**b**) Plots of the rate constants (k_{obs}) vs. [KNO_3]. The i_{cat} and i_p values are reflected by the maximal current of corresponding CV measurements.

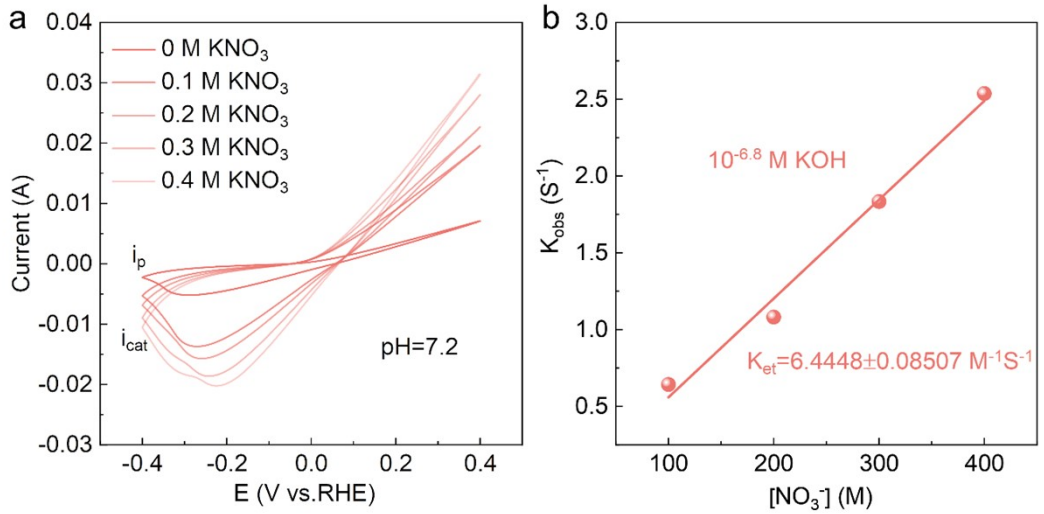

Figure S14. (**a**) CVs of the PA-CF with x M (x = 0, 0.1, 0.2, 0.3, 0.4) KNO_3 at pH=7.2. (**b**) Plots of the rate constants (k_{obs}) vs. [KNO_3]. The i_{cat} and i_p values are reflected by the maximal current of corresponding CV measurements.

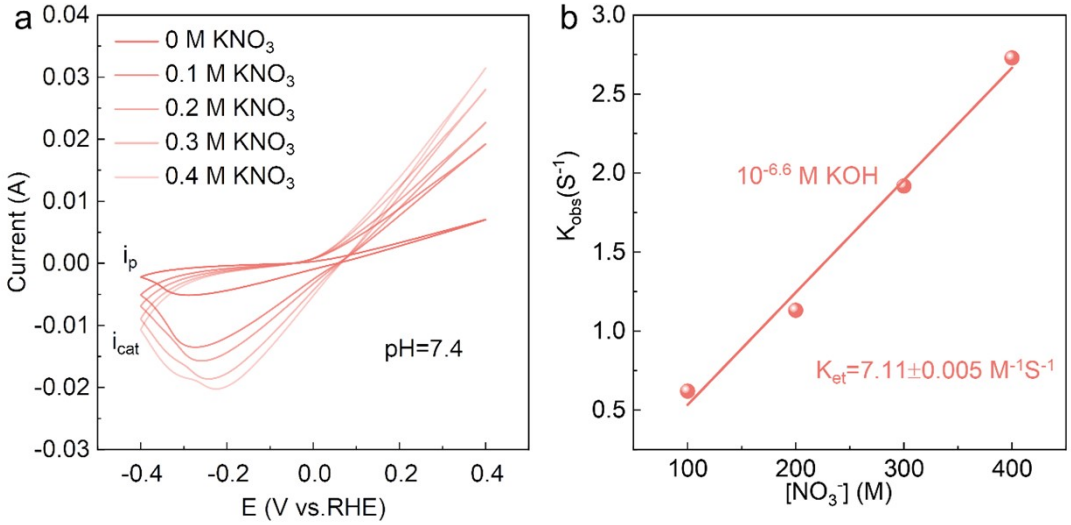

Figure S15. (**a**) CVs of the PA-CF with x M (x = 0, 0.1, 0.2, 0.3, 0.4) KNO_3 at pH=7.4. (**b**) Plots of the rate constants (k_{obs}) vs. [KNO_3]. The i_{cat} and i_p values are reflected by the maximal current of corresponding CV measurements.

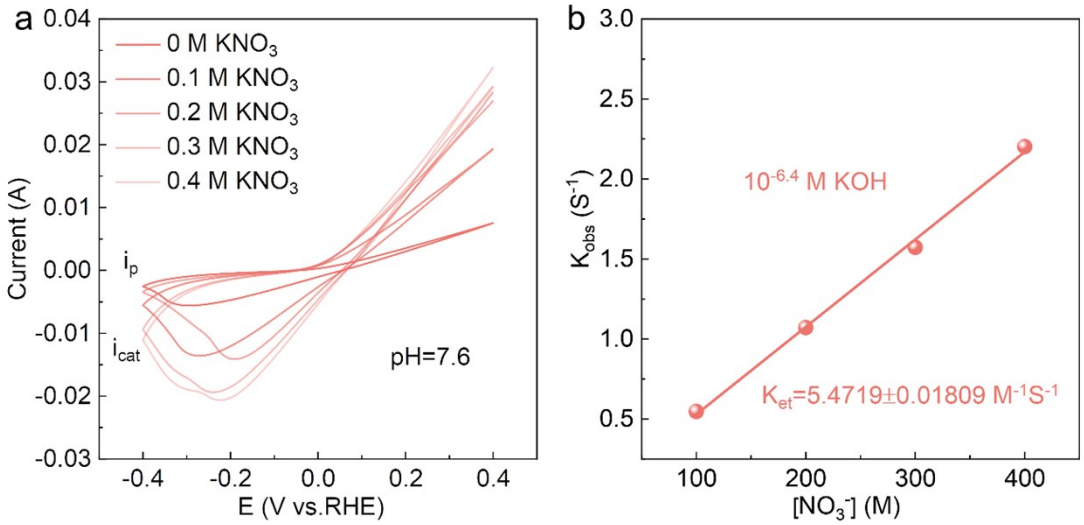

Figure S16. (a) CVs of the PA-CF with x M (x = 0, 0.1, 0.2, 0.3, 0.4) KNO_3 at pH=7.6. (b) Plots of the rate constants (k_{obs}) vs. [KNO_3]. The i_{cat} and i_p values are reflected by the maximal current of corresponding CV measurements.

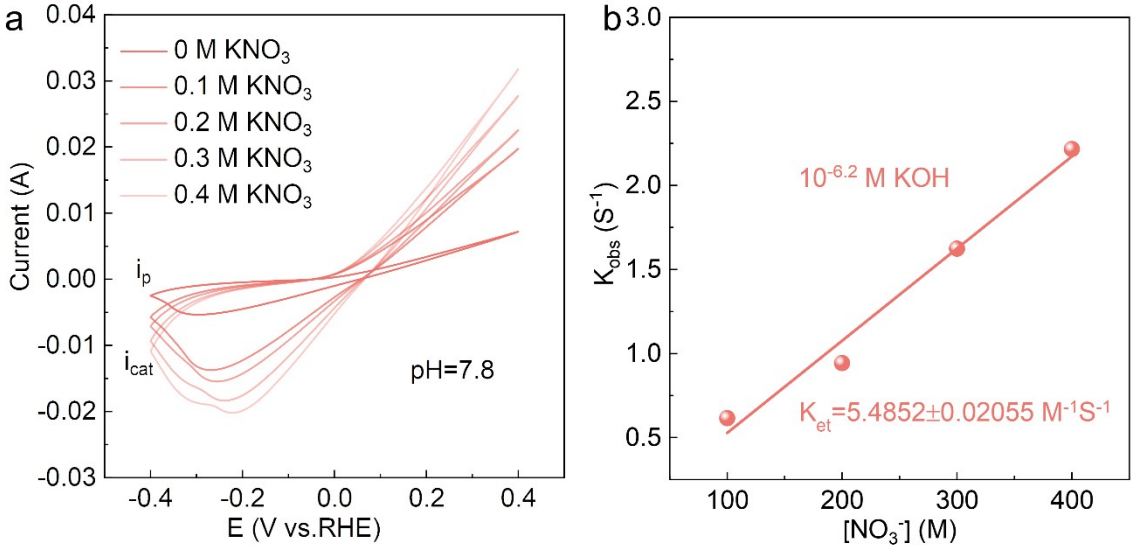

Figure S17. (**a**) CVs of the PA-CF with x M (x = 0, 0.1, 0.2, 0.3, 0.4) KNO_3 at pH=7.8. (**b**) Plots of the rate constants (k_{obs}) vs. [KNO_3]. The i_{cat} and i_p values are reflected by the maximal current of corresponding CV measurements.

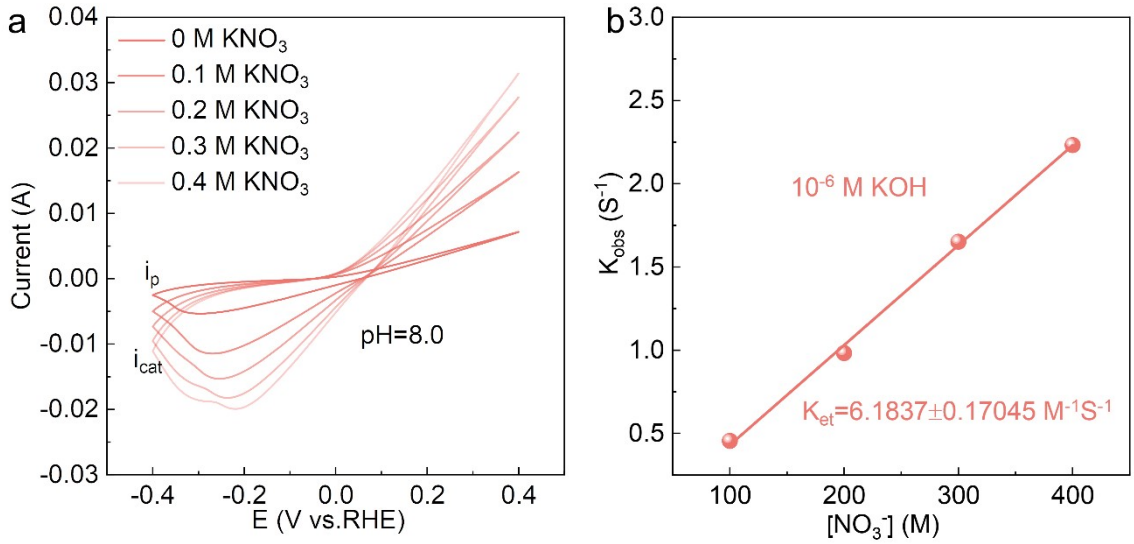

Figure S18. (**a**) CVs of the PA-CF with x M (x = 0, 0.1, 0.2, 0.3, 0.4) KNO_3 at pH=8.0. (**b**) Plots of the rate constants (k_{obs}) vs. [KNO_3]. The i_{cat} and i_p values are reflected by the maximal current of corresponding CV measurements.

pH	C_S (M)	k_{obs} (S^{-1})	k_{ET} ($M^{-1}\cdot S^{-1}$)	ΔG_{ET}^{0}(eV)
7	0.1	0.639561	6.09	0.83
	0.2	1.162729		
	0.3	1.8624		
	0.4	2.43519		
7.2	0.1	0.642577	6.44	0.8399
	0.2	1.081869		
	0.3	1.833669		
	0.4	2.53173		
7.4	0.1	0.619882	7.11	0.8499
	0.2	1.131376		
	0.3	1.917579		
	0.4	2.728576		
7.6	0.1	0.547423	5.47	0.86
	0.2	0.214301		
	0.3	1.57336		
	0.4	2.2025		
7.8	0.1	0.615756	5.49	0.8702
	0.2	0.944133		
	0.3	1.624676		
	0.4	2.216779		
8	0.1	0.454624	6.18	0.8806
	0.2	0.982396		
	0.3	1.651573		
	0.4	2.2325		

Figure S19. Summary of the parameters during k_{ET} and ΔG_{ET}^{0}.

Table S1. Comparison of the NH_3 electrosynthesis performance and energy consumption of PACF catalysts with those of the state-of-the-art Cu-based catalysts.

Catalyst	Operation Condition [V vs. RHE]	Electrolyte	r_{amm} [mmol h^{-1} cm^{-2}]	FE_{amm} [%]	Ref.
PA-CF	−0.4	0.2 M K_2SO_4+0.5 M KNO_3	0.55	~95.0	This Work
Ni_1Cu-SAA	−0.55	0.5 M Na_2SO_4+0.2 M NO_3^-	0.3267	~100.0	Ref. 12
Cu_2O	−0.559	0.5 M Na_2SO_4+0.2 M NO_3^-	0.24	85.3	Ref. 13
$LF_{0.9}Cu_{0.1}$	−0.9	0.5 M Na_2SO_4+0.05 M NO_3^-	0.0380	48±2	Ref. 14
TiO_2 NTs/ CuO_x	−0.75	0.5 M Na_2SO_4+0.1 M KNO_3	0.073	92.3	Ref. 15
CoP-Ni_2P	−0.9	0.5 M Na_2SO_4+0.49 mM KNO_3	0.0977	84.27	Ref. 16
Cu-cis-N_2O_2 SAC	−1.6	0.5 M K_2SO_4+9.89 mM KNO_3	1.69	80	Ref. 17
1-Cu	−0.9	0.5 M Na_2SO_4+5 mM $NaNO_3$	0.066	85.5	Ref. 18
RuO_2	−0.35	0.5 M Na_2SO_4+1.97 mM KNO_3	0.1158	97.46	Ref. 19
Rh@Cu-0.6%	−0.2	0.1 M Na_2SO_4+0.1 M KNO_3	1.27	93	Ref. 20
Cu/Cu_2O NWAs	−0.85	0.5 M Na_2SO_4+14.3 mM KNO_3	0.2449	95.80	Ref. 21
Cu/Pd/CuOx	−0.642	0.5 M K_2SO_4+0.49 mM KNO_3	0.0444	84.04	Ref. 22
Pd-Cu_2O CEO	−0.642	0.5 M K_2SO_4+0.49 mM KNO_3	0.0544	96.56	Ref. 21
CuO@PANI/CF	−0.642	0.5 M K_2SO_4+1.97 mM KNO_3	0.213	93.88	Ref. 23
FeN_2O_4 SAC	−0.88/−0.68	0.1 M K_2SO_4+0.5 M KNO_3	13.529	92.0	Ref. 24
FeMo SAC	−0.45	0.2 M K_2SO_4+0.05 M KNO_3	0.245	94.30	Ref. 25
Cu-N-C SAC	−1.0	0.5 M Na_2SO_4+1.97 mM $NaNO_3$	0.0380	48 ± 2	Ref. 26

Table S2. The Cu leaching of the PA-CF during 20 h of NITRR.

Total electrolyte volume (mL)	Electrolyte volume for ICP-MS (mL)	volume for ICP-MS (mL)	Measured content (ppm)	Mass of leached Cu in electrolyte (mg)	Mass of Cu in PA-CF (mg)	Cu loss (%)
50	3	10	2.06	0.10	100.1	0.10

Table S3. The fitted parameters of the EIS data of CF and PA-CF for NH_3electro synthesis.

Catalysts	η[mV]	R_s[Ω]	T[F s^{n-1}]	R_1[Ω]	n_1	R_2[Ω]	C_φ [F]
CF	0	4.223	0.000851	79.36	0.77799	67547.6	0.000226
	-30	4.261	0.000753	88.28	0.786	44943.8	0.000226
	-60	4.252	0.000744	91.51	0.78628	27126.2	0.000268
	-90	4.245	0.000762	88.15	0.78962	15227.5	0.000293
	-120	4.262	0.000738	78.14	0.80147	8768.3	0.000325
	-150	4.265	0.000755	73.03	0.80566	4378.4	0.000344
	-180	4.269	0.000763	67.19	0.8117	2095.8	0.00036
	-210	4.272	0.000763	61.09	0.81908	1093.6	0.000374
	-240	4.284	0.000748	54.07	0.82911	782.5	0.000393
	-270	4.322	0.000641	42.35	0.85731	425.8	0.000404
	-300	4.337	0.000575	34.73	0.87764	158.5	0.000391
PA-CF	0	3.304	0.006056	24.7	0.85072	3375.0	0.0057131
	-30	3.277	0.005368	14.09	0.80595	912.8	0.0036295
	-60	3.291	0.004696	8.789	0.81959	231.7	0.0036766
	-90	3.293	0.004358	6.366	0.83002	87.9	0.0033089
	-120	3.288	0.004029	4.718	0.84167	48.8	0.0028877
	-150	3.26	0.003755	1.861	0.84202	27.8	0.00032578
	-180	3.252	0.003522	2.277	0.85437	10.6	0.00090448
	-210	3.237	0.003242	1.947	0.86399	3.9	0.0017884
	-240	3.217	0.002931	1.56	0.87196	2.15	0.0018125
	-270	3.206	0.002664	1.381	0.88591	1.2	0.003499
	-300	3.185	0.002401	1.088	0.89241	0.8	0.0023447

References

1. W. Qiao, I. Waseem, G. Shang, D. Wang, Y. Li, F. Besenbacher, H. Niemantsverdriet, C. Yan and R. Su, *ACS Catal.*, 2021, **11**, 13510-13518.

2. S. Wang, K. Uwakwe, L. Yu, J. Ye, Y. Zhu, J. Hu, R. Chen, Z. Zhang, Z. Zhou, J. Li, Z. Xie and D. Deng, *Nat. Commun.*, 2021, **12**, 7072.
3. Y. Zhao, C. Liu, C. Wang, X. Chong and B. Zhang, *CCS Chem.*, 2021, **3**, 507-515.
4. C. Costentin, S. Drouet, M. Robert and J.-M. Savéant, *J. Am. Chem. Soc.*, 2012, **134**, 11235-11242.
5. C. Costentin and J. M. Savéant, *ChemElectroChem*, 2014, **1**, 1226-1236.
6. P. G.-B. Matthew J. Chalkley*†, Jonas C. Peters, *Science*, 2020, **369**, 850–854
7. P. Comba, S. Fukuzumi, H. Kotani and S. Wunderlich, *Angew. Chem. Int. Ed.*, 2010, **49**, 2622-2625.
8. H. K. Yong-Min Lee, Tomoyoshi Suenobu, Wonwoo Nam, and Shunichi Fukuzumi, *J. Am. Chem. Soc.*, 2008, **130**, 434-435.
9. E. Alsema, *Practical Handbook of Photovoltaics*, 2012, 1097-1117.
10. H. Kotani, S. Kaida, T. Ishizuka, M. Sakaguchi, T. Ogura, Y. Shiota, K. Yoshizawa and T. Kojima, *Chem. Sci.*, 2015, **6**, 945-955.
11. H. Kotani, H. Shimomura, K. Ikeda, T. Ishizuka, Y. Shiota, K. Yoshizawa and T. Kojima, *J. Am. Chem. Soc.*, 2020, **142**, 16982-16989.
12. J. Cai, Y. Wei, A. Cao, J. Huang, Z. Jiang, S. Lu and S.-Q. Zang, *Appl. Catal. B-Environ.*, 2022, **316**, 121683.
13. Z. Gong, W. Zhong, Z. He, Q. Liu, H. Chen, D. Zhou, N. Zhang, X. Kang and Y. Chen, *Appl. Catal. B-Environ.*, 2022, **305**, 121021.
14. K. Chu, W. Zong, G. Xue, H. Guo, J. Qin, H. Zhu, N. Zhang, Z. Tian, H. Dong, Y.-E. Miao, M. B. J. Roeffaers, J. Hofkens, F. Lai and T. Liu, *J. Am. Chem. Soc.*, 2023, **145**, 21387-21396.
15. W. Qiu, X. Chen, Y. Liu, D. Xiao, P. Wang, R. Li, K. Liu, Z. Jin and P. Li, *Appl. Catal. B-Environ.*, 2022, **315**, 121548.
16. Y. Gao, K. Wang, C. Xu, H. Fang, H. Yu, H. Zhang, S. Li, C. Li and F. Huang, *Appl. Catal. B: Environ.*, 2023, **330**, 122627.
17. X. F. Cheng, J. H. He, H. Q. Ji, H. Y. Zhang, Q. Cao, W. J. Sun, C. L. Yan and J. M. Lu, *Adv. Mater.*, 2022, **34**, 2205767.
18. Y.-T. Xu, M.-Y. Xie, H. Zhong and Y. Cao, *ACS Catal.*, 2022, **12**, 8698-8706.
19. J. Li, C. Zhang, C. Zhang, H. Ma, Z. Guo, C. Zhong, M. Xu, X. Wang, Y. Wang, H. Ma and J. Qiu, *Adv. Mater.*, 2022, **34**, e2203900.

20. H. Liu, X. Lang, C. Zhu, J. Timoshenko, M. Rüscher, L. Bai, N. Guijarro, H. Yin, Y. Peng, J. Li, Z. Liu, W. Wang, B. R. Cuenya and J. Luo, *Angew. Chem. Int. Ed.*, 2022, **61**, e202202556.
21. Y. Wang, W. Zhou, R. Jia, Y. Yu and B. Zhang, *Angew. Chem. Int. Ed.*, 2020, **59**, 5350-5354.
22. Y. Zhao, Y. Liu, Z. Zhang, Z. Mo, C. Wang and S. Gao, *Nano Energy*, 2022, **97**, 107124.
23. T. Ren, Z. Yu, H. Yu, K. Deng, Z. Wang, X. Li, H. Wang, L. Wang and Y. Xu, *Appl. Catal. B-Environ.*, 2022, **318**, 121805.
24. W.-D. Zhang, H. Dong, L. Zhou, H. Xu, H.-R. Wang, X. Yan, Y. Jiang, J. Zhang and Z.-G. Gu, *Appl. Catal. B-Environ.*, 2022, **317**, 121750.
25. E. Murphy, Y. Liu, I. Matanovic, S. Guo, P. Tieu, Y. Huang, A. Ly, S. Das, I. Zenyuk, X. Pan, E. Spoerke and P. Atanassov, *ACS Catal.*, 2022, **12**, 6651-6662.
26. J. Yang, H. Qi, A. Li, X. Liu, X. Yang, S. Zhang, Q. Zhao, Q. Jiang, Y. Su, L. Zhang, J.-F. Li, Z.-Q. Tian, W. Liu, A. Wang and T. Zhang, *J. Am. Chem. Soc.*, 2022, **144**, 12062-12071.